

Surface Chemistry

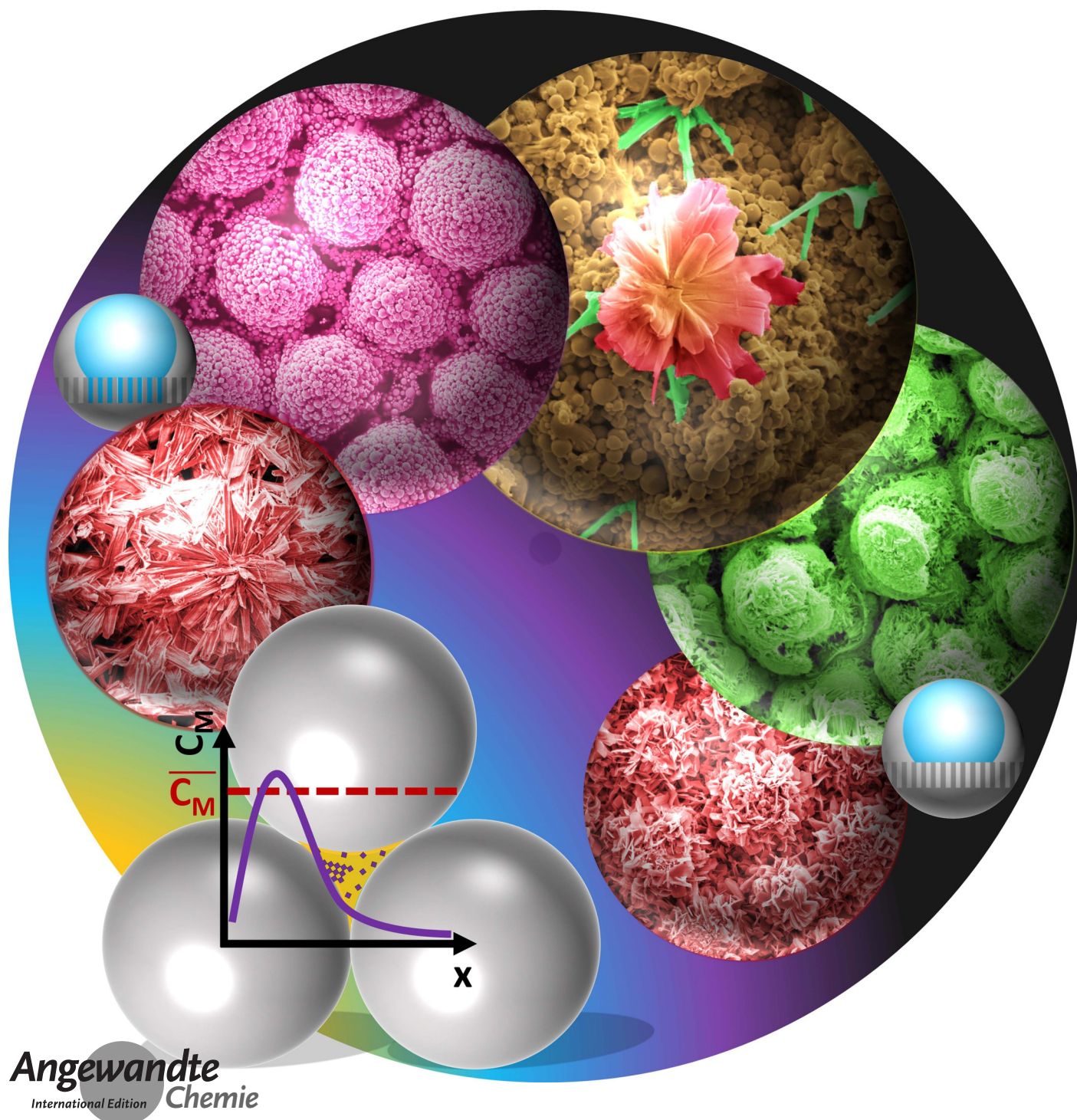
How to cite: *Angew. Chem. Int. Ed.* **2021**, *60*, 13929–13936

International Edition: doi.org/10.1002/anie.202101795

German Edition: doi.org/10.1002/ange.202101795

Tunable Hydrophobicity via Dimensionally Confined Polymerization of Organometallic Adducts

Julia J. Chang, Chuanshen Du, Alana Pauls, and Martin Thuo*



Angewandte
International Edition
Chemie

Abstract: Fabrication of tunable fine textures on solid metal surfaces often demands sophisticated reaction/processing systems. By exploiting *in situ* polymerization and self-assembly of inorganic adducts derived from liquid metals (the so-called HetMet reaction) with concomitant solidification, solid metal films with tunable texture are readily fabricated. Serving as a natural dimensional confinement, interparticle pores and capillary-adhered thin liquid films in a pre-packed bed of undercooled liquid metal particles lead to the expeditious surface accumulation of organometallic synthons, which readily oligomerize and self-assemble into concentration-dictated morphologies/patterns. Tuning particle size, particle packing (flat or textured), and reactant concentration generates diverse, autonomously organized organometallic structures on a metal particle bed. Concomitant solidification and sintering of the underlying undercooled particle bed led to a multiscale patterned solid metal surface. The process is illustrated by creating tunable features on pre-organized metal particle beds with concomitant tunable wettability as illustrated through the so-called petal and lotus effects.

Introduction

Hybrid organic-inorganic materials have emerged as a versatile synthetic materials platform on which new technologies are realized,^[1] albeit with underlying challenges in bonding.^[2] Resulting materials, however, exhibit distinct mechanical,^[3] thermal^[4] and electrical properties,^[5] with wide applications in biomedical,^[6] mechanics^[7] and heat-transferers.^[8] Metal- (MOF) and/or covalent- (COF) organic frameworks illustrates potential versatility in morphologies, topologies and compositions,^[9] powering interests in diverse fields such as phase separation,^[10] energy conservation^[11] and biomedical applications.^[12] These hybrid materials can be produced from self-assembly of polymer/inorganic nanoparticles.^[13] Commonly adopted batchwise solvothermal synthesis method is not amenable to generation of fine tunable surface features.^[14] In addition, fluctuating reactant concentration in a solvothermal process is not ideal for polymeri-


zation or uniform ad infinitum self-assembly which calls for steady-state kinetics.^[15] These challenges have been overcome through so-called heterogeneous metal-ligand (HetMet) reaction. In HetMet reaction, a metal ion reservoir is established as a liquid metal while a conjugate acid-base pair etch (H^+) and *in situ* chelate (B^-) the metal ions.^[16] Felicitous choice of reaction media sustains a saturated but dilute solution of the metal adduct resulting in ad infinitum polymerization and concomitant *in situ* assembly of organometallic adducts into high-aspect ratio structures.^[16a,b] The resulting material, however, are randomly dispersed in solution having no unique macro-assembly.


Dimensional confinements in precipitative reactions are potential tools in reigning macroscale assembly/organization of HetMet-derived organometallic structures with concomitant control over reaction kinetics and loci of the macro-assembly. For nucleation processes (crystallization or precipitative self-assembly), after reaching critical concentration, precursors accumulate at high-energy spots (impurities, defects, curvatures etc),^[17] followed by seed formation and growth. Dimensional confinement of the reaction media can therefore directly impact reaction rate, flux, and morphology of the products.^[18] For a chemical reaction $mA + nB \leftrightarrow pC + qD$, reaction rate, v , is determined by reactant concentration with the relation $v = k[A]^m[B]^n$. Local species concentration is, therefore, a critical parameter in engineering precipitation.

Granular packing of Undercooled Liquid Metal Core-Shell (ULMCS) particles and surface plasticity at the oxide-metal interface renders them ideal for dimensionally confined HetMet reactions. This plasticity implies that when v is low and/or particle is large, the reaction can be run for extended periods. When v is high, or particle is small ($\approx 1 \mu\text{m}$ diameter), continued depletion of oxide-especially where localized for example at capillary bridges, the protective oxide shell yields releasing the metastable liquid leading to sintering and solidification via heterogeneous nucleation.^[19a] Exploiting capillary effects to limit amount of reactant liquid on densified ULMCS particle bed enables tunable reactivity and accelerated reaction kinetics with solvent evaporation.^[19] These ULMCS particles beds are, therefore, exemplary platforms for studying dimensionally confined polymerization of inorganic polymeric materials for surface texturing.^[20] Tunability in particle size polydispersity, and therefore packing,^[21] renders ULMCS particles ideal building blocks for surface-bound organometallic ensembles of soft structures from HetMet reactions.^[19b,21]

Akin to other liquid metals, ULMCS particles are a good metal ion reservoir when subjected to a solution of conjugate acid-base pair (Figure 1 a). HetMet reaction leads to formation of organometallic structures that assemble into dispersed high-aspect ratio structures (Figure 1 b,c).^[16b] To exert dimensional confinement, a uniform multi-layer of ULMCS particles was pre-spincoated on ultra-flat Si (111) substrate (flat bed, Figure 1g) or pre-textured into periodic surface structures akin to a rose flower made via recently reported BIOMAP (biomimetic metal patterning) process (textured bed, Figure 1i).^[19b] When a small amount of conjugate acid-base pair solution is added to barely cover these beds, pores

[*] J. J. Chang, C. Du, A. Pauls, M. Thuo
Iowa State University, Department of Materials Science and Engineering
Ames, IA 50014 (USA)
E-mail: mthuo@iastate.edu
M. Thuo
Micro-Electronics Research Centre
Ames, IA 50014 (USA)
and
Iowa State University, Department of Electrical and Computer Engineering
Ames, IA 50014 (USA)

 Supporting information and the ORCID identification number(s) for the author(s) of this article can be found under:
<https://doi.org/10.1002/anie.202101795>.

 © 2021 The Authors. Angewandte Chemie International Edition published by Wiley-VCH GmbH. This is an open access article under the terms of the Creative Commons Attribution Non-Commercial NoDerivs License, which permits use and distribution in any medium, provided the original work is properly cited, the use is non-commercial and no modifications or adaptations are made.

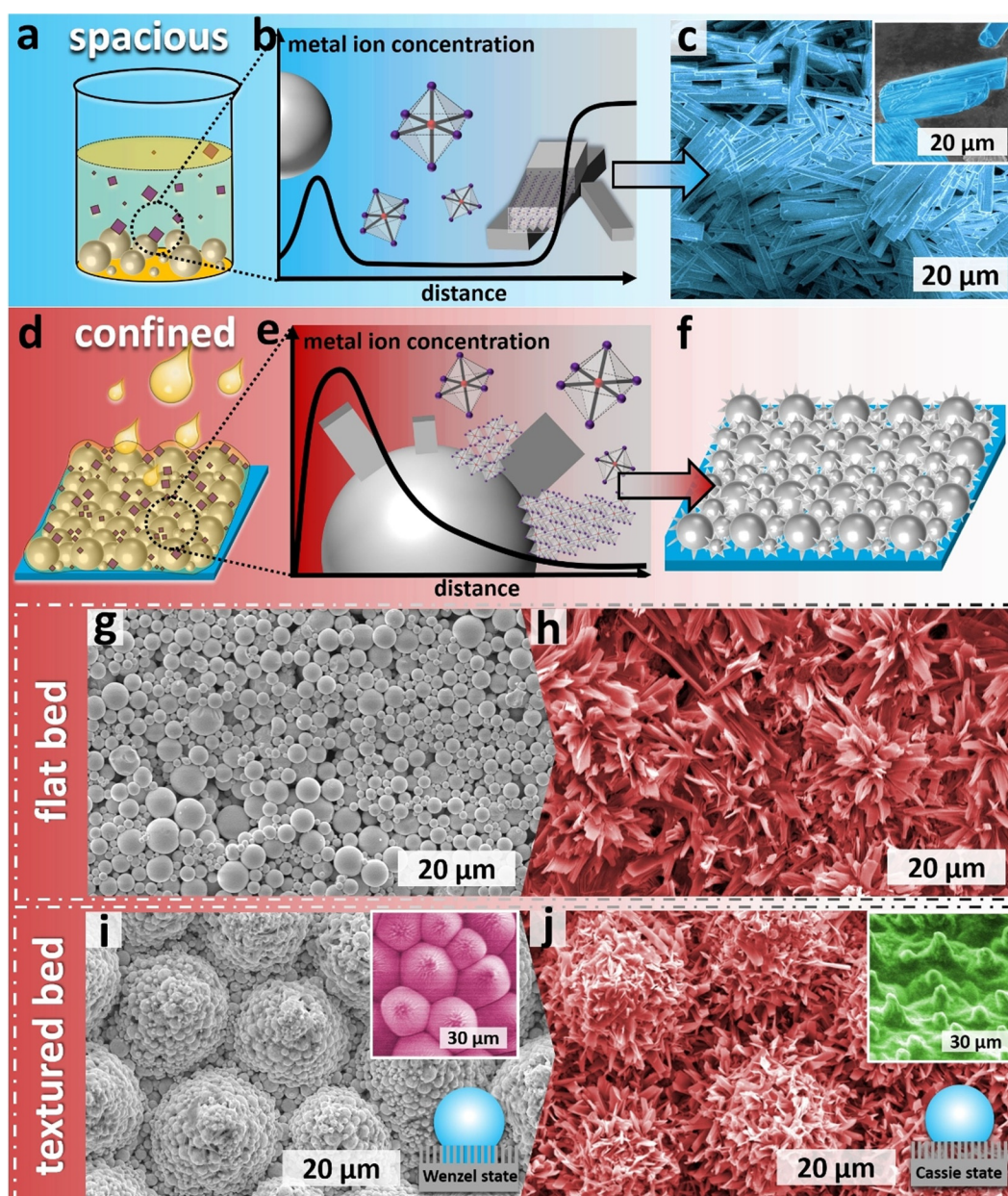


Figure 1. Schematic illustration and result summary of forming organometallic adducts by dimensionally confined polymerization. a) Polymerization of undercooled liquid Field's metal particles (HetMet reaction) in spacious synthesizing condition (e.g., solution). b) Relation between metal ion concentration with product generating distance of HetMet reaction. c) Formation of organometallic beams in the liquid phase. d) Scheme of confining HetMet reaction in the pores of particle assembly. e) Steep accumulation of metal ions resulting in rapid polymerization on particle surface. f) Cartoon of surface adducts formation upon particle bed. g) SEM image of flat undercooled liquid Field's metal particle bed. h) Organometallic adducts formation on surface of flat particle bed after treatment with 50% v/v acetic acid in ethanol solution. i) SEM image of textured undercooled liquid Field's metal particles with rose structure from BIOMAP process. Inset: analogous patterns on a fresh rose petal. j) Flower-like adducts formation on surface of textured particle bed after treatment with 50% v/v acetic acid in ethanol solution. Inset: multi-scale roughness on a fresh lotus.

and inter-particle spacing serve as dimensional confinement to generated adducts due to creation of capillary bridges with concomitant increase in wetted particle surface area (Figure 1 d). Adding acetic acid in ethanol solution onto particle assemblies, etched metal ion chelates (monomer synthons) accumulate in a low miscibility solvent leading to ad infinitum polymerization. Proximity to the particle surface induces on-particle deposition as the solvent evaporates (Figure 1 e). This ansatz implies that fine structures can be generated in situ by

dimensionally confined polymerization (Figure 1 f), either on flat (Figure 1 h) or textured particle bed (Figure 1 j). These adducts increase roughness on the particle beds, and like in natural self-cleaning systems, enable tunable wetting analogous to their biomimetic congeners^[22] ("Petal effect",^[23] Figure 1 i inset and "Lotus effect",^[24] Figure 1 j inset). We therefore infer, and demonstrate, that stoichiometric controlled growth of these organometallic adducts, and their autonomous self-assembly, extends the recently reported

metal soft-lithography BIOMAP fabrication method.^[19b] Akin to the lotus leaf, this introduction of multi-scale roughness should alter the nature of liquid contact line hence influence droplet pinning on fabricated surfaces. Herein, we investigate the role of enhanced tuning of wetting behavior on textured BIOMAP surfaces. We demonstrate the role of particle size, reaction rate, and particle bed organization on generated features and associated wetting characteristics of formed surfaces.

Results and Discussion

First, we investigate the effect of concentration of the conjugate acid-base pair on features formed on a flat particle bed. Undercooled Field's metal (51 % In, 32.5 % Bi and 16.5 % Sn w/w) core-shell particles were synthesized via the SLICE (Shearing Liquids Into Complex Particles) method.^[25] Particles of different size distributions were prepared by varying shear speed (Figure S1a–e).^[21] For a bed of particle-1 (Figure 2a) with average diameter, $d = 4.02 \pm 2.22 \mu\text{m}$ (Figure S1a), 25 % acetic acid in ethanol solution (v/v, 25-AcOH/EtOH) induced surface etching and precipitation as shown by contrast between carbon-rich (darker) regions on SEM images (Figure 2a_i). For clarity, the inset (Figure 2a_{ii}) shows a composite image of particle surfaces that have been exposed (yellow) and not exposed (blue) to the etchant. Contrast in surface morphologies between etched particle (rough, "Moon"-like) and an analogous pristine particle (smooth, "Uranus"-like) clearly illustrates deposition on the former.

Increasing the etchant concentration to 50 % v/v AcOH/EtOH generated exquisite surface-deposited organometallic polymer features ("polymer flowers") on the metal particle bed (Figure 2a_{iii}), composed of homogeneously distributed In, Sn, Bi as well as carbon and oxygen (Figure S2e). Increasing acid concentration (75 % v/v) enhanced growth and self-assembly leading to features with lower aspect ratio "petals" (Figure 2a_{iv}). We inferred that increase in concentration of etched metal adducts (organometallic monomers) favors rapid polymerization and accelerated self-assembly of the partially miscible adducts leading to a decrease in the aspect ratio. Capillary flow [Eq. (1)] and Washburn penetrativity, ($p = \gamma \cos \theta / 2\eta$ where η [MPa s] is viscosity of penetrating liquid)^[26] can be tuned via particle bed densification.^[21]

$$h = \frac{2\gamma \cos \theta}{\rho g r_0} \quad (1)$$

Where h [m] is the equilibrium liquid height, γ [mN m⁻¹] and θ [°] are liquid surface tension and its contact angle with channel wall, ρ is mass density [mg m⁻³], g is acceleration due to gravity [m s⁻²] and r_0 [m] is channel radius.^[27]

We therefore inferred that changing particle size will affect densification hence alter the kinetics of the HetMet reaction and associated self-assembly. To test this hypothesis, flat beds composed of particles of a variety of size distributions (particle 1–4, Figure S1a–S1d, Table S1) were treated with 25 %, 50 % and 75 % v/v AcOH/EtOH.

For particles with average size of $1.93 \pm 1.13 \mu\text{m}$ (particle-2, Figure 2b), no appreciable precipitation occurred after 25 % acid treatment. Capillary force generated during solvent evaporation, however, led to a more densely packed particle bed as captured by decrease in surface pores (Figure 2b_i). Increasing acid concentration to 50 % and 75 % v/v generated flower-like features analogous to those observed with particle-1 (Figure 2b_{iii} and b_{iv}, respectively). On further particle size reduction to $1.12 \pm 0.81 \mu\text{m}$ (Particle-3, Figure 2c), a small but continuous organometallic polymer layer was observed to be covering the assembly after 50 % -AcOH/EtOH treatment (Figure 2c_{iii}). In contrast, and as expected, a preserved smooth surface is obtained after 25 % -AcOH/EtOH treatment (Figure 2c_i). Raising acid concentration to 75 % v/v generated flowers with even high aspect ratio "petals" (Figure 2c_{iv}). Further decreasing the particle size to $0.75 \pm 0.46 \mu\text{m}$, however, prohibited the formation of flower-like features even when treated with 75 % AcOH/EtOH solution (Figure 2d_i–d_{iv}). We infer that this is likely due to reduced penetrativity hence poor bathing of the particles with the etchant, leading to significantly reduced etching hence reduced growth of surface precipitates. These results indicate a physical-chemical structural control of a surface reaction and self-assembly of resulting adducts.

To understand the effect of top-layer particle packing on adduct formation, particles sizes from flat-particle-bed SEM images were measured (Figure 2a_i, b_i, c_i and d_i). The slight, but statistically insignificant, decrease in average diameters of particles on top layer of assemblies compared to particles in as-prepared solution are likely due to self-filtration during the assembly formation (Figure S1f).^[28] This self-filtration is clearly captured in the insets of Figure 2d_i–d_{iv}. Top layer of flat beds from particle-1 and -2 showed a normal distribution in particle diameter (Figure 2e,f) indicating a stochastic distribution, but the smaller ones, particle-3 and -4, were better fitted to a lognormal function in part due to significant positive skew in the distributions (Figure 2g,h). This positive skew in size distribution, can affect packing and densification (Figure 2i, also see SI).^[28] This inference is informed by the fact that, for hard spherical granular matter, the packing factor, $\Phi = 0.634 + c_1 \delta + c_2 S \delta^2$ (where δ = polydispersity, S = skewness in particle size distribution, $c_1 = 0.0658$ and $c_2 = 0.0857$).^[29] The packing factor (densification) relates to porosity ($1 - \Phi$), hence we anticipate that a large skew and associated large polydispersity will lead to significant densification and much reduced porosity. Given that ULMCS particles are soft (non-Hertzian) and likely to be deformed to elliptical-like shapes under capillary pressure, a much higher densification is expected.^[21]

Figure 2j shows an increase in packing factor, Φ , with concomitant decreasing porosity, with decrease in particle size and increase in skewness. From Jurin's law [Eq. (1)] we infer that engineering densification, hence porosity, affects inter-particle distances and available void space (dimensions of fluid channels) which leads to rapid filling of the channel (low r) albeit with a small amount of the reactant solution. The more distributed a small amount of the fluid is, the lower the local concentration of the requisite organometallic synthons hence poor self-assembly. It is therefore expected

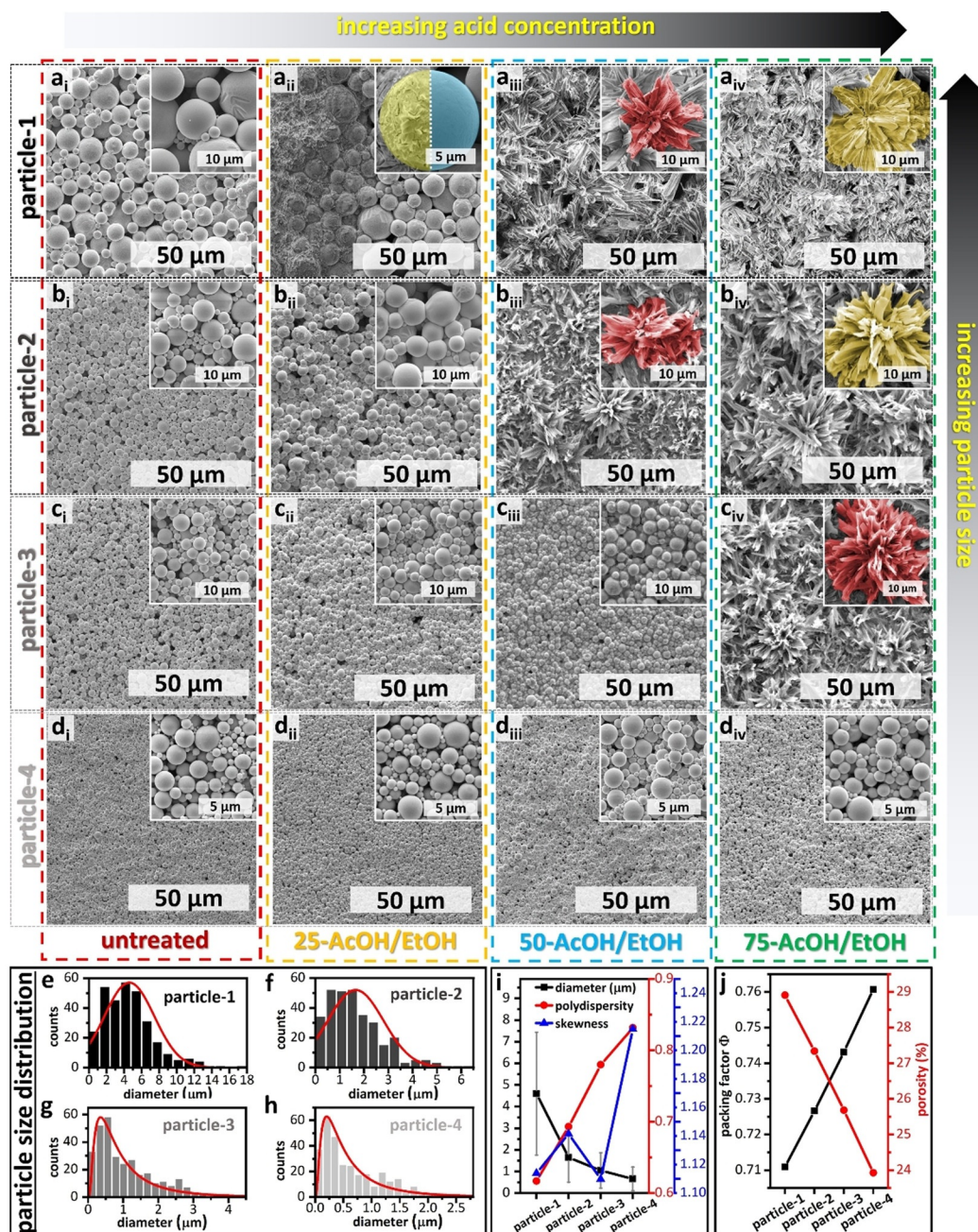


Figure 2. Effect of acidic solution concentration and particle size on surface precipitated organometallic structures formed on a flat layer of undercooled liquid Field's metal particles. Insets: false-coloured images of the dominant repeating feature on the surface. Data from similar particles sizes are presented in rows while those from same treatment are presented in columns. a) Untreated flat particle-1 bed and after 25% (a_{ii}), 50% (a_{iii}), 75% (a_{iv}), volume ratio acetic acid in ethanol solution (labelled 25-AcOH/EtOH, 50-AcOH/EtOH, 75-AcOH/EtOH, respectively). Similarly treated particle-2 ($b_{\text{i-iv}}$), particle-3 ($c_{\text{i-iv}}$) and particle-4 ($d_{\text{i-iv}}$). e–h) Histograms of particle size distribution of the top layer on flat beds of particles 1–4. i) Summary of diameter, skewness, and polydispersity of particle size distribution of the top layer particles captured in histograms given in (e)–(h). j) Inverse correlation of packing factor and porosity of flat particle beds.

that precipitated adducts will decrease with increase in penetration depth which correlates with enhanced densification as shown in Figure 2. This implies that a combination of particle packing and resulting capillary effects can be used to tune the rate of the HetMet reaction. Besides the distribution of the acid-base pair solution, and local concentration, smaller particles have higher curvature hence high strain and

associated Laplace pressure (ΔP). The increased surface stress may increase reactivity of the surface oxide, but this enhanced reactivity (stress relaxation) is frustrated by concentration of the requisite acetate conjugate acid-base pair.

A key tenet of the recently reported BIOMAP metal-based soft lithography with undercooled metal particles,^[19b] is concomitant phase change. We observed characteristic spi-

nodal decomposition from partially polymerized ULMCS (Figure S2a,b),^[30] and anticipated significant changes in conductivity upon solidification and sintering since interparticle space in non-connected particle is dominated by organic surface ligands. Metallic connectivity will show Ohmic conductivity (linear $I-V$ curve), while presence of organic adducts introduces tunneling components (sigmoidal $I-V$ curve) or non-Ohmic charge carriers in otherwise highly conductive system. We therefore anticipate two major changes in charge transport, *viz*; i) a change from a sigmoidal to linear $I-V$ curve, and ii) increased conductivity as we move from wide non-Hertzian contacts in liquid particles to sintered solid metal, albeit via thin (necks) connections. Obtained $I-V$ curves of the particle beds before and after acid treatment, as expected, show a change in the shape of the $I-V$ curve and about five orders of magnitude increase ($\approx 3 \mu\text{A}$ to 100mA) in conductivity (Figure S2c,d). We can therefore infer that, as previously observed,^[19a,21] the resulting surface structures are formed on solid metal surfaces although built on the liquid nature of ULMCS particles.

Having shown the dependency of generated features on the surface area in contact with the reactants, we desired to enhance the contact by creating a particle bed that enhances accessible contact area with the reactant solution. The recently reported rose-flower templated surface offer such a system.^[19b] For brevity and clarity, we compare textured surfaces derived from the largest (particle 1) and smallest (particle 4) particles. For particle-1 (average diameter = $4.02 \mu\text{m}$), higher structural porosity due to large particle size induced in situ polymerization during the BIOMAP process (Figure 3a). Geometric confinement in the PDMS mold used to create the patterns implied that features formed during the BIOMAP process were poorly ordered (Figure 3a, see inset

for zoom in). We observe fine hair-like nanostructures on the surface of these particles, indicating limited growth of the organometallic adducts. A 25% AcOH/EtOH treatment produced needle-shaped surface structures (Figure 3b) unlike in analogous non-patterned particle bed (Figure 2a_{ii}). Increasing acid concentration led to increased growth of these features (Figure 3b–d) without change in morphology. For particle-4 (average diameter = $0.75 \mu\text{m}$), BIOMAP, as expected, led to a metal rose structure without texturing, in part due to reduced penetrativity and high densification (Figure 3e). A 25% AcOH/EtOH solution treatment induced growth and surface self-assembly, creating a composite mixture of “flower-like” (composed of small sheet-like features) and “grass-like” (composed of small wire/beam-like features) polymers on the structured particle surface (Figure 3f). Increasing acid concentration to 50% AcOH/EtOH led to domination by the flower-like features (Figure 3g) analogous to those observed with flat particle beds (Figure 2b_{iii/c_{iv}}) albeit with slight differences in dimensions. Further increase in acid concentration to 75% AcOH/EtOH, however, led to disordered surface deposition with concomitant loss in the petal-like topology (Figure 3h). We infer that the higher surface area and high acid concentration led to over etching of the material resulting in stochastic precipitation of the large quantities of the organometallic adducts. We infer that a balance between surface area, particle packing/densification, and acid concentration (here 50% AcOH/EtOH for particle-4) is needed for controlled composition, etching, in situ polymerization of organometallic adducts, and surface self-assembly into a new ordered texture (Figure S3).

Apart from direct microscopy imaging of polymeric adducts, contactless profilometer was applied to capture changes in surface profiles of metallic rose-like features from

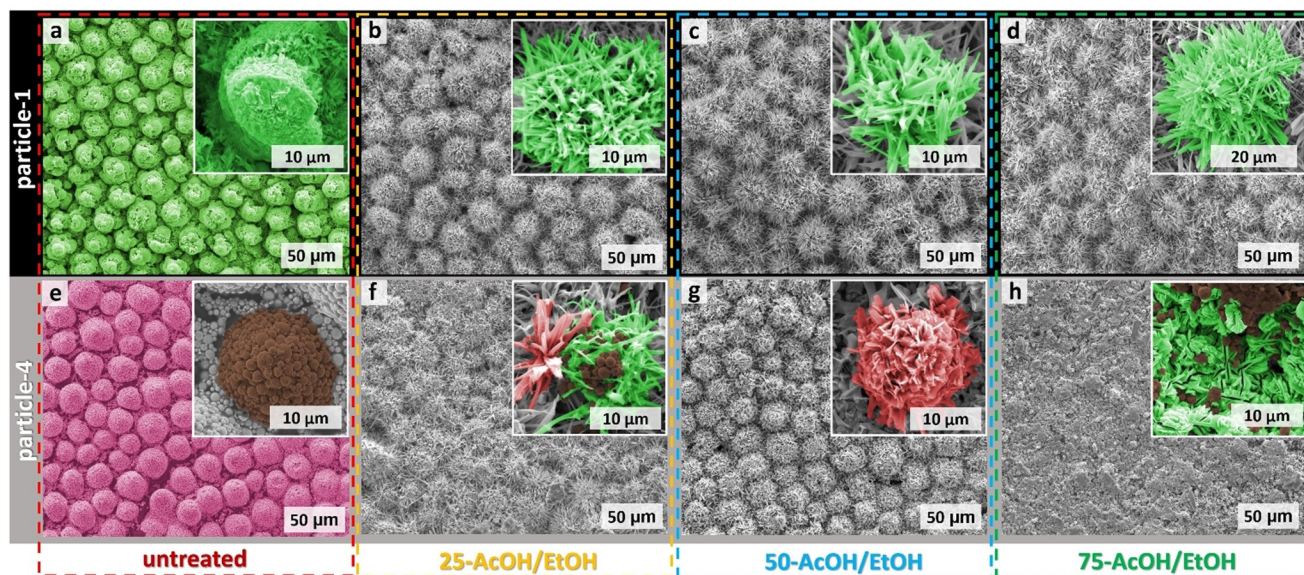


Figure 3. Effect of acidic concentration and particle size on organometallic structure formation on textured undercooled liquid Field's metal particles (metal rose). a) In-situ polymerization during the fabrication of textured particle-1 bed. b) Effect of 25% v/v acetic acid in ethanol solution (25-AcOH/EtOH) on textured particle-1 bed. c) 50% v/v AcOH/EtOH (50-AcOH/EtOH) acidic solution treated textured particle-1 bed. d) 75% v/v-AcOH/EtOH (75-AcOH/EtOH) acidic solution treated textured particle-1 bed. e–h) Untreated, 25%, 50%, or 75%-AcOH/EtOH acidic solution treated textured particle-4 bed.

particle-4 (Figure 4a, from sample in Figure 3e) and composite textured features created from particle-1 (Figure 4b, from Sample in Figure 3a). Figure 4b showed significantly large asperities (length along z-axis), which we infer to be due to surface deposition of the organometallic polymer adducts.

To evaluate the effect of the generated surface texturing on surface properties, hydrophobicity was investigated using a goniometer equipped with a tilting base and a medium speed (35 flames⁻¹) camera. Wetting behavior were compared to those of the rose petal and the lotus leaf (16 day old leaf—see Figure S4) to differentiate droplet adhesion (petal effect) or lack thereof (lotus effect). Compared to clean metallic replica of the rose petal pattern (Figure 3e, contact angle $129.8 \pm 5.5^\circ$), in situ textured assembly of particle-1 (composite lotus, Figure 3a) gave a contact angle, $\theta = 143.2 \pm 5.4^\circ$. This is a significant increase in non-wetting properties ($\Delta\theta = 13.4^\circ$) approaching the super-hydrophobic regime (Figure 4c). With such high contact angles, we evaluated stickiness of water droplets by placing a droplet on a 30° (Figure 4d) or 60° (Figure 4e) tilted surface. We observe that unlike in the rose-replica, the droplets roll off the tilted composite surface indicating a Lotus effect compared to the pinning (Petal effect) observed with the metallic rose pattern replica (see

supporting video 1).^[19b] These results confirm that even tighter dimensional confinement during the organometallic polymerization, herein enhanced by the PDMS mold, is a feasible approach to create highly hydrophobic surfaces (Figure 4c). Further grafting organometallic adducts on the surface of the composite surface (treated composite lotus-like), however, leads to loss ($\Delta\theta = -25.9^\circ$) in hydrophobicity (Figure 4c) likely due to loss of the hair-like surface features and likely loss of hierarchical multi-scale texture. An analogous observation was made with the pre-organized powder derived from smaller particles (particle-4, Figure 3e vs. g) where a decrease in hydrophobicity ($\Delta\theta = -27.7^\circ$) was observed with texturing. We infer that precise multiscale morphology control of surface deposited organometallic polymeric feature is critical in achieving desired wetting properties.

Conclusion

In conclusion, we demonstrated dimensional confined in situ organometallic polymerization of adducts derived from undercooled liquid metal particles to form tuneable surface fine structures. Concomitant sintering and solidification of the metal particle bed leads to a textured solid metal surface irrespective of the particle assembly geometry. This texture tuning approach is therefore applicable to both flat (2D) or 3D ordered undercooled metals assemblies, upon which various surface features could be generated with change in wetting (and tribological) properties. Felicitous choice of particle size, hence densification, affects fluid flow rates and penetrativity. Denser packing of the particles, therefore, results in decreased metal-organic monomer concentration thus favors high aspect ratio polymeric features. By demonstrating wetting states from Wenzel (petal effect) to Cassie (lotus effect), we infer that the reported approach is amenable to surface property tuning.

Acknowledgements

This work was supported by Iowa state university. The authors thank Dr. Warren Straszheim (SEM) for technical assistance.

Conflict of interest

The authors declare no conflict of interest.

Keywords: polymerization · self-assembly · textured surfaces · undercooled metals · wetting

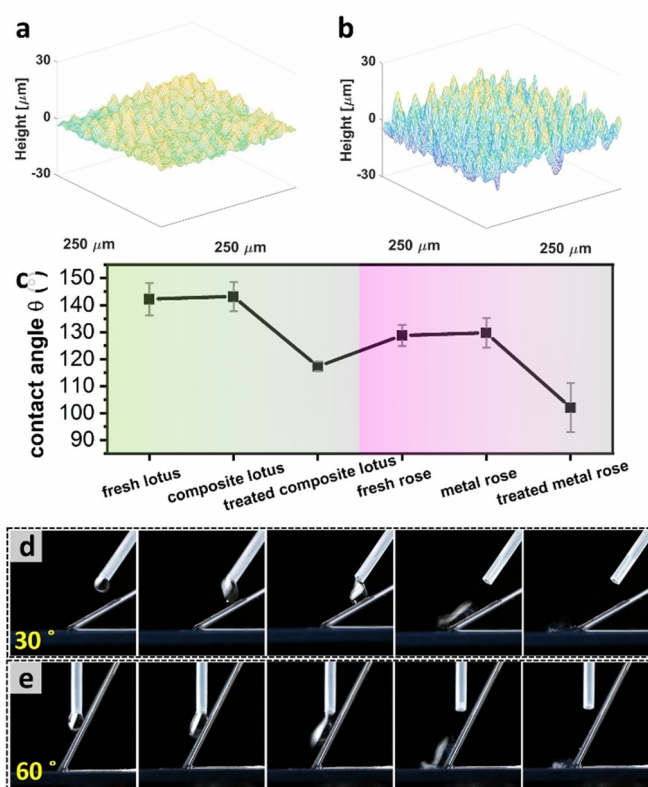


Figure 4. Lotus effect on composite lotus from a metal rose base. a) Surface profile of metal rose like patterns derived from particle 4. b) Surface profile of composite lotus leaf like patterns from particle -1. c) Contact angle of fresh lotus leaf, untreated metallic composite lotus leaf analogy and 50-AcOH/EtOH treated textured bed (treated composite lotus) of particle-1 as well as fresh rose petal, untreated (metal rose) and 50-AcOH/EtOH treated textured bed (treated metal rose) of particle-1. Water droplets rolling off the composite lotus surface when tilted d) 30° or e) 60° degrees.

- [1] a) B. J. Blaiszik, S. L. Kramer, S. C. Olugebefola, J. S. Moore, N. R. Sottos, S. R. White, *Annu. Rev. Mater. Res.* **2010**, *40*, 179–211; b) Z.-M. Dang, J.-K. Yuan, J.-W. Zha, T. Zhou, S.-T. Li, G.-H. Hu, *Prog. Mater. Sci.* **2012**, *57*, 660–723; c) H. Qian, E. S. Greenhalgh, M. S. Shaffer, A. Bismarck, *J. Mater. Chem.* **2010**, *20*, 4751–4762; d) U. G. Wegst, H. Bai, E. Saiz, A. P. Tomsia, R. O. Ritchie, *Nat. Mater.* **2015**, *14*, 23–36.

- [2] a) B. S. Chang, R. Tutika, J. Cutinho, S. Oyola-Reynoso, J. Chen, M. D. Bartlett, M. M. Thuo, *Mater. Horiz.* **2018**, *5*, 416–422; b) M. Shahinpoor, K. J. Kim, *Smart Mater. Struct.* **2001**, *10*, 819.
- [3] M. Shahinpoor, K. J. Kim, *Smart Mater. Struct.* **2004**, *13*, 1362.
- [4] X. Xu, J. Chen, J. Zhou, B. Li, *Adv. Mater.* **2018**, *30*, 1705544.
- [5] G. Yun, S.-Y. Tang, S. Sun, D. Yuan, Q. Zhao, L. Deng, S. Yan, H. Du, M. D. Dickey, W. Li, *Nat. Commun.* **2019**, *10*, 1300.
- [6] a) H. Palza, *Int. J. Mol. Sci.* **2015**, *16*, 2099–2116; b) M. Shahinpoor, K. J. Kim, *Smart Mater. Struct.* **2004**, *14*, 197.
- [7] a) M. Aureli, V. Kopman, M. Porfiri, *IEEE ASME Trans. Mechatron.* **2009**, *15*, 603–614; b) S. M. Mirvakili, I. W. Hunter, *Adv. Mater.* **2018**, *30*, 1704407.
- [8] H. Chen, V. V. Ginzburg, J. Yang, Y. Yang, W. Liu, Y. Huang, L. Du, B. Chen, *Prog. Polym. Sci.* **2016**, *59*, 41–85.
- [9] a) Y. V. Kaneti, J. Tang, R. R. Salunkhe, X. Jiang, A. Yu, K. C. W. Wu, Y. Yamauchi, *Adv. Mater.* **2017**, *29*, 1604898; b) Q.-L. Zhu, Q. Xu, *Chem. Soc. Rev.* **2014**, *43*, 5468–5512.
- [10] a) J. E. Bachman, Z. P. Smith, T. Li, T. Xu, J. R. Long, *Nat. Mater.* **2016**, *15*, 845–849; b) T. Rodenas, I. Luz, G. Prieto, B. Seoane, H. Miro, A. Corma, F. Kapteijn, F. X. L. i Xamena, J. Gascon, *Nat. Mater.* **2015**, *14*, 48–55.
- [11] a) Z. Liang, C. Qu, W. Guo, R. Zou, Q. Xu, *Adv. Mater.* **2018**, *30*, 1702891; b) Y. Xu, Q. Li, H. Xue, H. Pang, *Coord. Chem. Rev.* **2018**, *376*, 292–318.
- [12] D. Giliopoulos, A. Zamboulis, D. Giannakoudakis, D. Bikiaris, K. Triantafyllidis, *Molecules* **2020**, *25*, 185.
- [13] N. J. Penfold, J. Yeow, C. Boyer, S. P. Armes, *ACS Macro Lett.* **2019**, *8*, 1029.
- [14] N. Stock, S. Biswas, *Chem. Rev.* **2012**, *112*, 933–969.
- [15] I. Luz, A. Loiudice, D. T. Sun, W. L. Queen, R. Buonsanti, *Chem. Mater.* **2016**, *28*, 3839–3849.
- [16] a) B. S. Chang, A. Martin, B. Thomas, A. Li, R. W. Dorn, J. Gong, A. J. Rossini, M. M. Thuo, *ACS Mater. Lett.* **2020**, *2*, 1211–1217; b) B. S. Chang, B. Thomas, J. Chen, I. D. Tevis, P. Karanja, S. Çınar, A. Venkatesh, A. J. Rossini, M. M. Thuo, *Nanoscale* **2019**, *11*, 14060–14069; c) A. Martin, C. Du, B. Chang, M. Thuo, *Chem. Mater.* **2020**, *32*, 0.
- [17] a) J. J. De Yoreo, P. G. Vekilov, *Rev. Mineral. Geochem.* **2003**, *54*, 57–93; b) P. G. Vekilov, B. R. Thomas, F. Rosenberger, *J. Phys. Chem. B* **1998**, *102*, 5208–5216.
- [18] S. A. McBride, R. Skye, K. K. Varanasi, *Langmuir* **2020**, *36*, 11732.
- [19] a) A. Martin, B. S. Chang, Z. Martin, D. Paramanik, C. Frankiewicz, S. Kundu, I. D. Tevis, M. Thuo, *Adv. Funct. Mater.* **2019**, *29*, 1903687; b) J. J. Chang, A. Martin, C. Du, A. M. Pauls, M. Thuo, *Angew. Chem. Int. Ed.* **2020**, *59*, 16346–16351; *Angew. Chem.* **2020**, *132*, 16488–16493.
- [20] a) B. S. Chang, M. Fratzl, A. Boyer, A. Martin, H. C. Ahrenholtz, I. De Moraes, J.-F. Bloch, N. M. Dempsey, M. M. Thuo, *Ind. Eng. Chem. Res.* **2019**, *58*, 4137–4142; b) S. Çınar, I. D. Tevis, J. Chen, M. Thuo, *Sci. Rep.* **2016**, *6*, 1–12; c) A. Martin, W. Kiarie, B. Chang, M. Thuo, *Angew. Chem. Int. Ed.* **2020**, *59*, 352–357; *Angew. Chem.* **2020**, *132*, 360–365.
- [21] A. Martin, C. Du, A. M. Pauls, T. Ward III, M. Thuo, *Adv. Mater. Interfaces* **2020**, *7*, 2001294.
- [22] J. Long, P. Zhou, Y. Huang, X. Xie, *Adv. Mater. Interfaces* **2020**, *7*, 2000997.
- [23] L. Feng, Y. Zhang, J. Xi, Y. Zhu, N. Wang, F. Xia, L. Jiang, *Langmuir* **2008**, *24*, 4114–4119.
- [24] a) Y. T. Cheng, D. Rodak, C. Wong, C. Hayden, *Nanotechnology* **2006**, *17*, 1359; b) A. Marmur, *Langmuir* **2004**, *20*, 3517–3519; c) N. A. Patankar, *Langmuir* **2004**, *20*, 8209–8213.
- [25] I. D. Tevis, L. B. Newcomb, M. Thuo, *Langmuir* **2014**, *30*, 14308–14313.
- [26] E. W. Washburn, *Phys. Rev.* **1921**, *17*, 273.
- [27] P.-G. de Gennes, F. Brochard-Wyart, D. Quéré, *Capillarity and wetting phenomena*, Springer, Heidelberg, **2004**, pp. 33–67.
- [28] S. D. Kulkarni, B. Metzger, J. F. Morris, *Phys. Rev. E* **2010**, *82*, 010402.
- [29] K. W. Desmond, E. R. Weeks, *Phys. Rev. E* **2014**, *90*, 022204.
- [30] R. Ball, R. Essery, *J. Phys. Condens. Matter* **1990**, *2*, 10303.

Manuscript received: February 4, 2021

Accepted manuscript online: February 18, 2021

Version of record online: April 1, 2021